International Journal of Advancements in Communication Technologies– IJACT
Volume 1 : Issue 3 *[ISSN 2374-1511]*
Publication Date : 27 December,2014

SENSOSOL: MultiFOV 4-Quadrant high precision sun sensor for satellite attitude control

J. M. Quero, P. Castro, J. M. Moreno, M. Reina, P. Ortega

***Abstract*—The design, manufacturing and calibration of an improved miniaturized two axis sun sensor for satellite attitude control is presented, including the manufacturing process using MEMS technologies. The high precision is obtained by the subdivision of the field of view (FOV). The FOV and the resolution obtained are ±60º and 0.5º for the coarse measure and ±35º with precision better than 0.1º for the fine measure.**

***Keywords*— angle measurement, microelectromechanical system (MEMS), microsensors, photodiodes, sun sensor, MultiFOV, SENSOSOL, attitude control.**

I. Introduction

A sun sensor is a device used to measure the incidence angle of sun rays with respect to a reference surface. Typical applications of sun sensors are the attitude control of satellites and space vehicles [1], the control of solar power plants [2], or the smart control of air-conditioning in vehicles. Sun sensors can be classified as digital [3] [4] or analog [5] [6] depending on the kind of manufacturing technology and coarse or fine depending on the accuracy of the measurement. While coarse sun sensors get typically 1 degree of accuracy, fine sun sensors reach up to 0.01 degrees.

An analog sun sensor consists of several optoelectronic modules. The most important one is the optical sensing component, able to convert the optical information, provided by the sun rays, in electrical current or voltage. These signals usually are low powered, so one or more amplification stages are needed in order to get both reliable and easy to handle signals. Additionally, more stages can be used to adapt them to an appropriate format, for instance to a proper range of voltages.

Our research group has been developing sun sensors in satellite and industrial applications for fifteen years, and several designs are being used now in different applications [7] [8] [10]. The basic structure of all these analog sun sensors is composed of sensing elements, implemented with photodiodes and an operational amplifier, used to convert the currents generated by each photodiode into voltage.

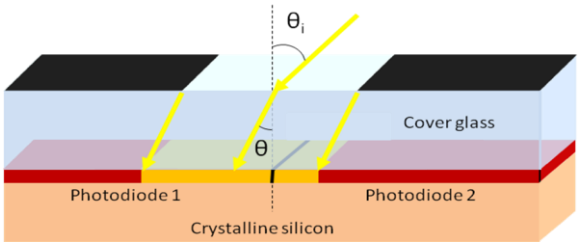

Figure 1. Structure of a sensing element.

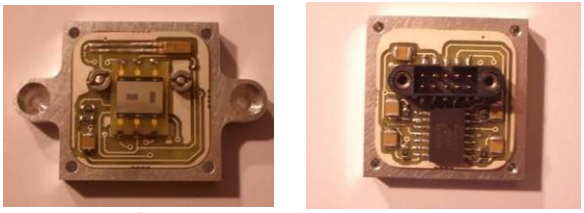

a) b)

Figure 2. Real implementation of the Vectorsol sun sensor.

Fig. 1 shows the structure of a sensing element. Two photodiodes are implemented in a silicon p-doped bulk. The sun rays reach the photodiodes through a cover glass with an upper window generating current in each one.

From the current ratio we can obtain the incidence angle of the incoming ray.

A real implementation of an analog sun sensor is shown in Fig. 2. This sun sensor, Vectorsol [9], was designed to be onboard as scientific payload in the Spanish satellite Nanosat 1B, launched in July of 2009. The sensing element (in the center of the left figure) is composed by four photodiodes, grouped two-by-two, implementing a two axis sensor. The sensing element is placed in a printed circuit board where the rest of the discrete electronic elements are placed too. Approximated dimensions of the PCB are 25x25 mm^2.

II. Vectorsol Description

A. *Sensing elements*

Vectorsol sensor consists of two pairs of photodiodes which are orthogonally placed in order to measure the angle in both axes. Fig. 3 shows the two axes of the sun sensor layout and the manufactured silicon die, including the cover glass window. The alignment between cover glass and silicon has been optically done using the alignment marks in the window.

J. M. Quero, P. Castro, J. M. Moreno
Universidad de Sevilla
Spain
quero@us.es

M. Reina
Instituto Nacional de Técnica Aeroespacial
Spain

P. Ortega
Universidad Politécnica de Cataluña
Spain

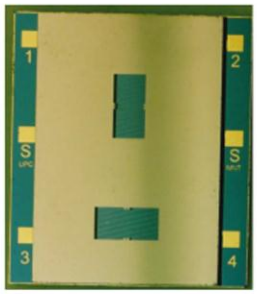

Figure 3. Fabricated silicon dice and cover glass.

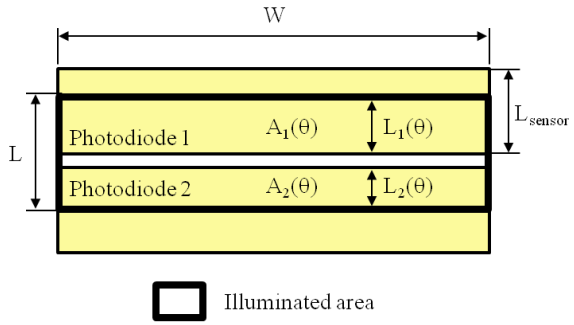

Figure 4. Illuminated area in two photodiodes.

For each axis, given the illuminated area of the photodiodes (Fig. 4), it is possible to determine the angle of incidence using (1).

$$R(\theta) = \frac{I_{ph_2} - I_{ph_1}}{I_{ph_2} + I_{ph_1}} = \frac{A_2(\theta) - A_1(\theta)}{A_2(\theta) + A_1(\theta)} = \frac{L_2(\theta) - L_1(\theta)}{L_2(\theta) + L_1(\theta)} \quad (1)$$

Where $L_1 \cdot W$ and $L_2 \cdot W$ are the illuminated area of the photodiodes 1 and 2, respectively. The normalized function guarantees the independence of R with the radiation intensity.

B. *Calibration process*

Once the device is manufactured, a calibration process is needed. The sensor is illuminated with a fixed solar simulator and the rotation in both axes is accurately controlled by two motorized rotary stages.

For each angular position, the voltage is measured and the R function is calculated. By combining the R function of the two axes it is possible to obtain the inverse function ($\theta_{x,y}=f(R_1,R_2)$).

During the normal operation of the sensor, the value of R in both axes is calculated and applied into the inverse function obtaining the angular position [9]. A linear interpolation is done using the three nearest points in the plot.

III. Sensosol 4-Quadrant Design

The topology of the new sensor uses a single structure instead of two separated pairs of photodiodes (Fig. 5). In order to obtain the measures in both axes, the generated currents in the photodiodes are added two by two. This structure is more compact due to the size reduction and more robust since there are no internal reflections and the measures in both axes are obtained using the same photodiodes.

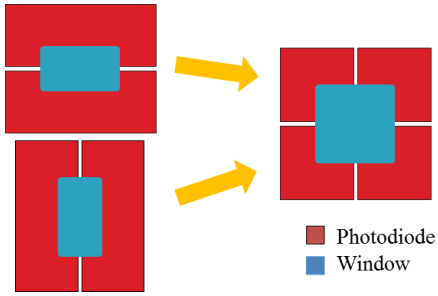

Figure 5. New 4-Quadrant structure.

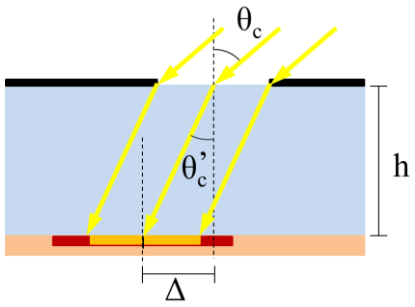

Figure 6. Displacement of the window.

By increasing the height of the glass layer, it is possible to manufacture a more accurate sensor. On the other hand, increasing the height implies decreasing the FOV: one single sensor is capable to see only a narrow region.

The complete FOV will be reached by adding four sensors in the same device. In order to obtain complementary regions of the FOV, it is necessary to modify the central angle of the sensors (the incidence angle of the incoming ray in which the four photodiodes are equally illuminated). To achieve this, the upper window is displaced (Fig. 6).

The complete device is composed by 5 sensors (Fig. 7, Fig. 8): one of them is used as fine sensor (C), with a ±35º FOV and the other four are used as coarse sensor (A, B, D, and E), each of them controlling one quarter of the complete FOV.

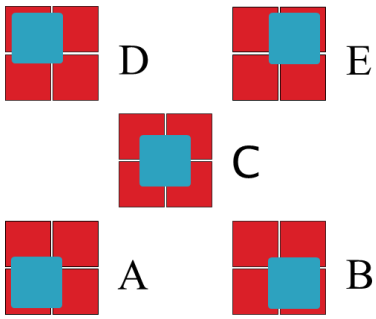

Figure 7. Complete sensor design.

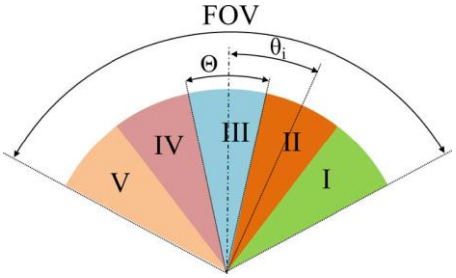

Figure 8. Subdivision of the FOV.

IV. Fabrication using MEMS Technology

In previous Vectorsol sensor, the bonding process of the borofloat and the silicon die makes use of alignment marks in the windows metal mask and in the silicon chip to align both elements using a microscope. It is a very tedious process and gives non repetitive alignment errors. The improvement of the alignment accuracy has been done by manufacturing an alignment frame using MEMS and SU8 techniques (Fig. 9) using the BETTS process [10].

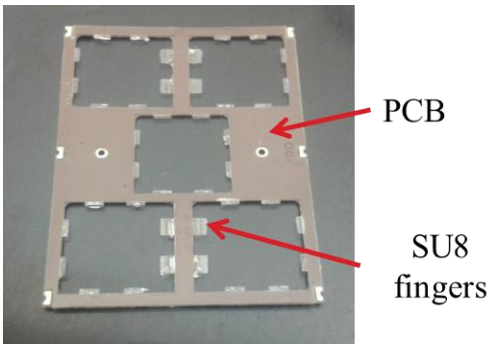

Figure 9. Alignment frame.

The estimated alignment error using this technique is about 20 µm on displacement and less than 0.05º on rotation. The same design of the PCB manufactured for the alignment frame (without the SU8) is used as optical isolation between sensors on the final device.

In Figure 10, the intermediate fabrication steps are presented: a) five silicon dies bonded to the substrate PCB, b) borofloat shields bonded on top of the silicon dies, c) an auxiliary PCB used as optical isolation between sensor and d) the final device.

In Figure 10(d), it can be seen an additional metalized glass layer, which is used to avoid the entrance of non-desired light beams through the lateral sides of the borofloat.

This device is placed on a PCB containing the signal adaptation circuit. The whole structure is encapsulated using an aluminum shell (Fig. 11).

To perform the ADC conversion and the digital signal processing, there is an auxiliary unit with a FPGA which makes all the computation and also stores calibration tables (Fig. 12).

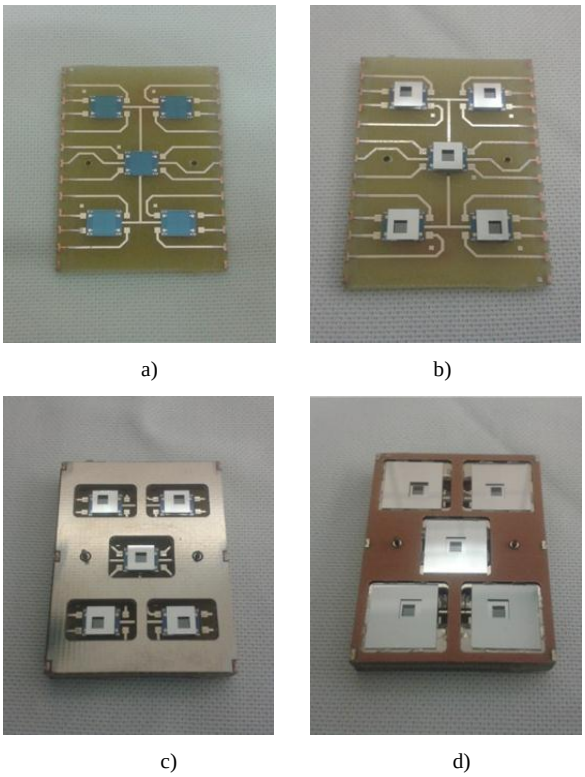

Figure 10. Fabrication steps: a) five silicon dies bonded to the substrate PCB, b) borofloat shields bonded on top of the silicon dies, c) an auxiliary PCB used as optical isolation between sensor and d) the final device.

Figure 11. SENSOSOL sensing unit.

Figure 12. SENSOSOL processing unit.

v. Space Qualification.

In order to qualify SENSOSOL for space applications it has been subjected to different environmental test. All these test were done in the facilities of the Instituto Nacional de Técnica Aeroespacial (INTA) by highly qualified and experienced staff.

A. Vibration test

Vibration test is intended to prove that SENSOSOL endure severe vibrations that will receive during the launch. SENSOSOL has been submitted to vibrations up to 30g and 2 kHz frequency.

In fig. 13 can be seen SENSOSOL processing unit fixed to a shaker just before z axis vibration test.

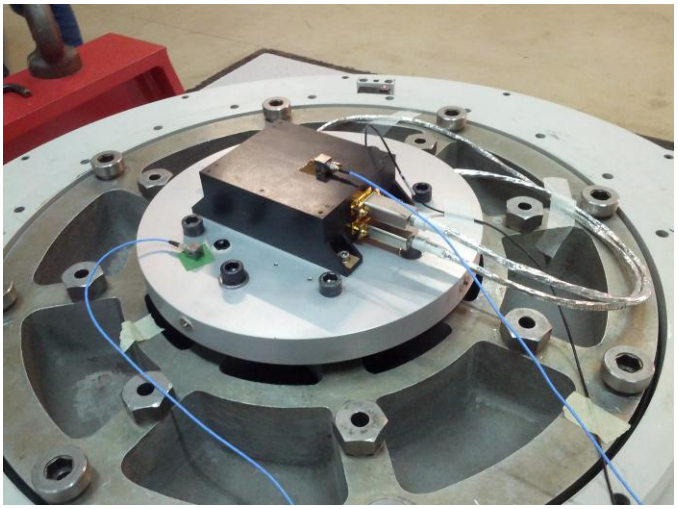

Figure 13. SENSOSOL Z axis vibration test.

B. Thermal Vacuum test

Thermal vacuum test is necessary to check SENSOSOL behavior and normal operation in vacuum situation and in extreme temperatures.

SENSOSOL has been tested in a temperature range of [-60, +110] ºC with a vacuum pressure better than 10^{-6} mbar, demonstrating that it can work in space environmental conditions successfully.

C. EMC Test

SENSOSOL was also submitted to Electromagnetic Emissions and Electromagnetic Susceptibility tests, both conducted and radiated, accomplishing the general requirements for mission payloads.

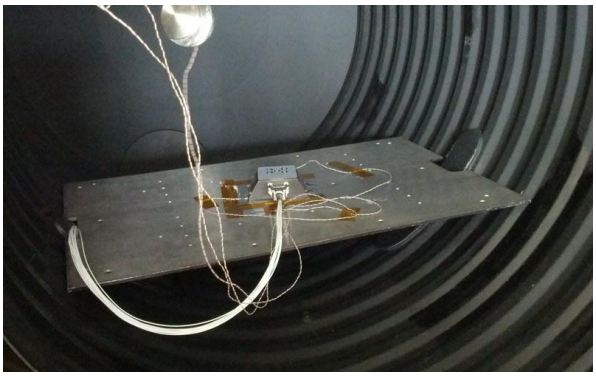

Figure 14. Climatic chamber thermal vacuum test.

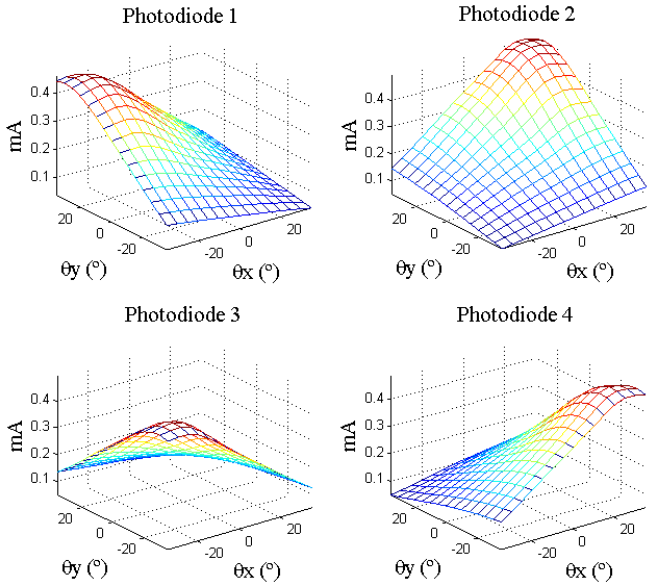

Figure 15. Generated photocurrents in sensor C.

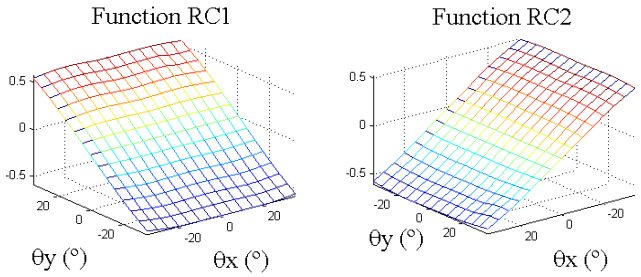

Figure 16. R functions in sensor C.

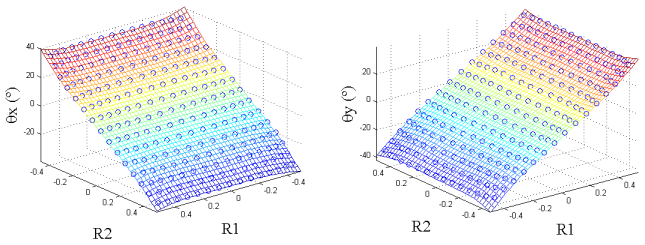

Figure 17. Inverse functions in sensor C.

VI. Experimental Results

A calibration of ±60º with a 5º steps in both axes has been performed, as shown in Fig. 15 and Fig. 16. The generated photocurrent in each photodiode as a function of incident angles for both axes is represented, as well as the R functions for the central sensor (sensor C, ±35º).

Each sensor is using the information collected in their region. The plots for the four peripherals sensors are similar but displaced to the correspondent operating region.

In Fig. 17 the inverse functions for the sensor C ($\theta_{x,y}=f(RC_1,RC_2)$) can be seen. In addition, the interpolated surfaces (used to obtain angles between calibration points) are represented in the plots.

Once the calibration curve is obtained, a verification process is necessary. The sensor response for 100 random positions in all the FOV are captured and compared with the real angles provided by the rotary stages. The calculated 3σ value for the coarse measure and the fine one is shown in Table 1.

TABLE I. 3σ VALUES FOR BOTH AXES IN ALL THE FOV

Measure	Sensor	3σ X axis (º)	3σ Y axis (º)
Fine	C (FOV ±6º)	0.042	0.043
	C (FOV ±35º)	0.149	0.148
Coarse	A, B, D, E	0.491	0.507

VII. Conclusions

This paper showed the design, fabrication and characterization of a high precision solar sensor based on the subdivision of the FOV. A new 4-Quadrant structure has been used. Experimental results have been shown. The FOV and the resolution obtained are ±60º and 0.5º for the coarse measure and ±35º with precision better than 0.15º for the fine measure. In ±6º FOV it has a precision better than 0.05º.

This sensor, named SENSOSOL, will be on board as scientific payload of SEOSAT/INGENIO satellite, which is planned to be launched in 2015.

Acknowledgment

Author thanks MNT group of the Universidad Politécnica de Cataluña, where silicon dices were manufactured and the spin-off Solar MEMS Technologies, where the complete device where manufactured and evaluated. The described investigations were carried out within the research project SENSOSOL ACI-B-2011-0702 granted by the Ministerio de Ciencia e Innovación.

References

[1] P. Furgale, J. Enright, T. Barfoot, "Sun Sensor Navigation for Planetary Rovers: Theory and Field Testing," Aerospace and Electronic Systems, IEEE Transactions on Aerospace and Electronic Systems, vol.47, no.3, pp.1631-1647, July 2011.

[2] J. M. Quero, C. Aracil, L. G. Franquelo, J. Ricart, P. R. Ortega, M. Dominguez, L. Castañer, and R. Osuna, "Tracking Control System Using an Incident Radiation Angle Microsensor," IEEE Trans. Ind. Electron., vol. 54, no. 2, pp. 1207–1215, Apr. 2007.

[3] Young-Keun Chang, Seok-Jin Kang, Byung-Hoon Lee. "High-Accuracy Image Centroiding Algorithm for CMOS-based Digital Sun Sensors". IEEE Sensors 2007 conference. 329-336.

[4] Carl Christian Liebe. "Solar Compass Chip". IEEE Sensor Journal, vol. 4, nº 6, December 2004.

[5] Tobias Böhnke, Marika Edoff, Lars Stenmark. "Development of a MOEMS Sun Sensor for Space Applications". Sensors and Actuators A, 130-131 (2006), 28-36.

[6] Young-Keun Chang, Mi-Yeon Yun, Byung-Hoon Lee. "A New Modelling and Validation of Two-axis Miniature Fine Sun Sensor". Sensors and Actuators A, 134 (2007), 357-365.

[7] Patent of Universidad de Sevilla. "Sistema para el Posicionamiento de una Superficie Respecto del Sol Mediante dos Sensores Solares". Quero, José Manuel. ES. P200900206. January 26, 2009.

[8] F. J. Delgado, P. Ortega, C. L. Tarrida, J. García, M. Angulo, J. M. Quero, "A New Design of High Precision Solar Microsensor for Satellite Applications", Proc. of the 9th IEEE Conference on Sensors, Waikoloa, Hawaii, Nov. 1-4, 2010.

[9] P. Ortega, G. Lopez, J. Ricart, M. Dominguez, L. Castañer, J.M. Quero, C.L. Tarrida, J. García. "Fabrication of a Miniaturized Two Axis Sun Sensor for Satellite Applications". IEEE Sensors Journal, vol 10, nº10, pgs. 1623-1632, Oct. 2010.

[10] C. Aracil, F. Perdigones, J. M. Moreno, J. M. Quero. "BETTS: Bonding, exposing and transferring technique in SU-8 for microsystems fabrication". Journal of Micromechanics and Microengineering. vol. 20, pp. 8–13, feb. 2010.

[11] F. J. Delgado, J. García, J. M. Quero, C. L. Tarrida, P. Ortega, S. Bermejo. "Accurate and Wide Field of View MEMS-based Sun Sensor for Industrial Applications", IEEE Trans. Ind. Electron., vol. 59, no. 12, pp. 4871–4880, dec. 2012.